HHS Public Access

Author manuscript

Radiology. Author manuscript; available in PMC 2015 December 04.

Published in final edited form as:

Radiology. 2014 June ; 271(3): 633–652. doi:10.1148/radiol.14132232.

CT Angiography after 20 Years:

A Transformation in Cardiovascular Disease Characterization Continues to Advance[1]

Geoffrey D. Rubin, MD, **Jonathon Leipsic, MD**, **U. Joseph Schoepf, MD**, **Dominik Fleischmann, MD**, and **Sandy Napel, PhD**

[1]Duke Clinical Research Institute, 2400 Pratt St, Box 17969, Durham, NC 27715 (G.D.R.); Department of Medical Imaging and Division of Cardiology, University of British Columbia, Vancouver, BC, Canada (J.L.); Department of Radiology and Radiological Science, Medical University of South Carolina, Charleston, SC (U.J.S.); and Department of Radiology, Stanford University School of Medicine, Stanford, Calif (D.F., S.N.)

Abstract

Through a marriage of spiral computed tomography (CT) and graphical volumetric image processing, CT angiography was born 20 years ago. Fueled by a series of technical innovations in CT and image processing, over the next 5–15 years, CT angiography toppled conventional angiography, the undisputed diagnostic reference standard for vascular disease for the prior 70 years, as the preferred modality for the diagnosis and characterization of most cardiovascular abnormalities. This review recounts the evolution of CT angiography from its development and early challenges to a maturing modality that has provided unique insights into cardiovascular disease characterization and management. Selected clinical challenges, which include acute aortic syndromes, peripheral vascular disease, aortic stent-graft and transcatheter aortic valve assessment, and coronary artery disease, are presented as contrasting examples of how CT angiography is changing our approach to cardiovascular disease diagnosis and management. Finally, the recently introduced capabilities for multispectral imaging, tissue perfusion imaging, and radiation dose reduction through iterative reconstruction are explored with consideration toward the continued refinement and advancement of CT angiography.

The past 20 years have witnessed a remarkable transformation in the diagnosis and characterization of vascular disease. The 1990s were a particularly golden period in vascular diagnosis and therapy with the introduction of computed tomographic (CT) angiography, contrast material–enhanced magnetic resonance (MR) angiography, and endovascular repair of aortic aneurysms using stent-grafts.

Address correspondence to G.D.R. (grubin@duke.edu).

Disclosures of Conflicts of Interest: G.D.R. Financial activities related to the present article: none to disclose. Financial activities not related to the present article: HeartFlow stock options, granted more than 36 months prior to publication. Other relationships: none to disclose. **J.L.** Financial activities related to the present article: personal fees as a consultant to HeartFlow and GE Healthcare. Financial activities not related to the present article: none to disclose. Other relationships: none to disclose. **U.J.S.** Financial activities related to the present article: none to disclose. Financial activities not related to the present article: grants from Bayer, Bracco, GE, Medrad, and Siemens; travel paid by Bayer; institution received payment for preparation of educational materials from GE; workstations and software from Siemens and Medrad. Other relationships: none to disclose. **D.F.** Author stated no relevant conflicts of interest to disclose. **S.N.** Financial activities related to the present article: none to disclose. Financial activities not related to the present article: none to disclose. Other relationships: consultant to Carestream and advisory board for Fovia and EchoPixel.

In the early 1990s nearly every patient preparing to undergo vascular surgery, requiring confirmation of pulmonary embolism, or suspected of having traumatic aortic injury, intracranial aneurysm, or renovascular hypertension underwent conventional diagnostic angiography, a technique that was born in 1924 (1) and substantially refined to present-day technique with the introduction of the Seldinger guidewire in 1953 (2). Combined with steady improvements in injectors, film changers, and fluoroscopic, radiographic, and subtraction techniques, direct arteriography evolved as the reference standard for the diagnosis and characterization of all manner of vascular disease. Its strengths were a high spatial resolution and an opportunity for diagnosis and therapeutic intervention during a single session. Its limitations were the cost, discomfort, and risks of an invasive procedure, particularly when concurrent intervention was not indicated; inability to demonstrate the vessel wall, perivascular tissue, and end-organ parenchyma; poor three-dimensional (3D) spatial discrimination owing to the projectional nature of the acquisition; necessity for multiple contrast material injections and repeated doses of ionizing radiation to characterize spatial relationships; and downstream luminal opacification limited by selective arterial injection of contrast material.

Essentials

- Driven by profound technologic advances, CT angiography has emerged as the dominant imaging modality for diagnosis and planning management of vascular diseases.
- CT angiography has provided new insights into the pathophysiology and natural history of acute aortic syndromes.
- Optimized CT angiographic technique enables comprehensive assessment of peripheral arterial disease.
- The advancement of transcatheter cardiovascular therapies, including aortic stent-graft deployment and aortic valve implantation, are linked to insights provided by CT angiography.
- Innovations in CT technology are providing unprecedented opportunities to further enhance the safety and clinical value of CT angiography.

MR angiography, first reported in 1986 (3,4) was an exciting new technique that was dependent on flow-related enhancement, awaiting further technical improvements that would make it a mainstream diagnostic angiographic modality. At the same time, conventional CT, acquired with 10-mm-thick sections that were standard for the day (5), was viewed as a maturing technology, having made tremendous inroads into a broad spectrum of medical diagnoses, but was limited for the assessment of vascular disease with only one mainstream application, assessing aortic rupture risk by tracking the transverse dimension of abdominal aortic aneurysms.

Emergence of CT Angiography

The primary enabling technology for CT angiography was the clinical introduction of spiral (6) or helical (7) scanning in 1990, which ushered in the era of volumetric CT. Its key contribution was the replacement of the “step and shoot” acquisition mode, in which the table was static during the acquisition of a single transverse section and subsequently advanced to the next scan position before gantry rotation resumed, with continuous acquisition of projections during table travel that allowed coverage of much larger volumes per unit time. Among other advantages, this permitted the capture of the first pass of an intravenous contrast agent bolus as it transited a particular vascular territory. In those early days, table speed was limited to the section thickness per gantry rotation; thus, for example, given a 1-second gantry rotation and 3-mm sections, table speed was 3 mm/sec. Another limitation was x-ray tube heat capacity, limiting milliamperage (and, thereby, increasing noise) and scan time to less than 30 seconds, resulting in a maximum coverage with the same parameters of 9 cm (8).

The first articles describing CT angiography appeared in the November 1992 edition of *Radiology* (9,10) and demonstrated the possibilities given fast volume coverage and 3D visualization. From 1991 to 1998, single–detector row spiral CT technique limited clinical CT angiography to discrete vascular territories. Prior to the introduction of scan pitch values greater than one, a scan with 3-mm nominal section thickness provided a maximum of 9 cm table travel in 30 seconds and thus limited initial applications to the extracranial carotid arteries (10), the circle of Willis (11), the renal arteries (12,13) (Fig 1a), and the proximal abdominal aorta (13). While a nominal section thickness of 3 mm was considered maximal for the creation of useful multiplanar reformations and 3D renderings, early CT angiography pioneers effectively used the primary transverse reconstructions from spiral CT acquisitions with 5 mm thickness to evaluate the central pulmonary arteries (14) and the thoracic aorta (15). With the clinical introduction of scan pitch values between one and two (16), maximal anatomic coverage doubled, paving the way for an expansion in clinical applications, to include assessments of acute aortic syndromes (AAS), the detection of aortic injury in trauma patients, and the qualitative and quantitative characterization of the aorta as key enablers for planning aneurysm therapy. While many investigations focused on the refinement of the techniques for CT angiogram acquisition and postprocessing, new clinical insights were made possible by CT angiography’s ability to volumetrically resolve the entirety of the blood vessel lumen, wall, and end organ (14,17–22).

With the clinical potential for CT angiography established, the industry sought to further increase volume coverage through the development of scanners with faster gantry rotation and with multiple parallel detector rings that acquired more than one section per rotation. Early multi–detector row CT scanners introduced in 1998 had four detector rings and were capable of 1/2-second gantry rotations, effectively multiplying volume coverage per unit time ×8 at the same section thickness (8,23) (Fig 1b, 1c). Fifteen years later, today’s multidetector CT scanners have up to 320 detector rings, gantry rotation times as low as 270 msec, and in some cases two x-ray sources, allowing submillimeter isotropic resolution to be acquired over very large volumes in, at most, a few seconds. Faster volume coverage also

allowed a sizable reduction in contrast media usage without loss in vascular conspicuity (24).

With the introduction of multidetector CT, virtually all limits on longitudinal coverage disappeared, paving the way for CT angiography to be applied to imaging the inflow and run-off of the lower extremity arterial system (25), the entire cervicocranial vascular system (23), the thoracoabdominal aortoiliac system (23), and the upper extremity arterial system (26). By the year 2002, there was but one final arterial frontier remaining—the coronary arteries. While proof-of-concept investigations of coronary CT angiography were published using four- and eight-row multi-detector CT scanners (27), the introduction of 16-row multidetector CT brought coronary CT angiography to clinical practice and with 64-row multidetector CT in 2005 it became mainstream.

Computers and Image Processing

The rapid evolution of fast CT scanners is congruent with Moore's law, which predicts the doubling of the density of transistors on integrated circuits approximately every 2 years. In addition to effecting the acquisition circuitry, Moore's law is also responsible for the rapid increase in computer performance/price ratios, without which the expense and time to reconstruct these high-resolution cone-beam volume acquisitions, consisting of hundreds to thousands of sections, would not be clinically practical. Moore's law is also directly responsible for the final enabler of clinical CT angiography: Because section-by-section inspection of CT angiographic images is neither efficient nor intuitive, visualization of CT angiography studies employs shaded surface displays, maximum intensity projections, and volume rendering (Fig 1b, 1c). While early datasets consisted of only tens of cross-sections, each of the many desired view directions required many seconds to compute on expensive workstations. Today, many vendors provide software that runs on inexpensive computers and is capable of interactive high-resolution volume rendering with advanced lighting effects based on thousands of contrast-enhanced CT sections with additional capabilities such as automated bone removal and curved planar reformatting. The analysis of CT angiographic datasets has evolved to the point where review of the transverse reconstructions is a secondary analysis to tailored visualization and quantitation tasks using application-specific postprocessing solutions.

Contributions of CT Angiography to Clinical Practice

As a result of tremendous technologic developments, CT angiography has evolved to provide important insights into cardiovascular disease diagnosis and management. While there are many applications of CT angiography that have transformed the standard for clinical care and are worthy of detailed elaboration, we have chosen to focus specifically on three areas in which CT angiography has expanded our understanding of human vascular disease (AAS and peripheral arterial disease), in which it has guided new strategies in disease management (aortic endograft deployment and transaortic valve implantation), and in which new CT techniques offer promise for further refinements (coronary heart disease).

Acute Aortic Syndromes: New Knowledge Redefining Disease Classification

AAS refers to a spectrum of acute, life-threatening abnormalities of the aorta characterized by an abrupt onset of intense chest or back pain (28). CT angiography has not only revolutionized the diagnosis and management of cases of AAS (29), but when acquired with electrocardiographic (ECG) synchronization has fundamentally advanced our understanding of these conditions (30), becoming the preeminent technique for the diagnosis, characterization, and treatment planning of AAS. In addition to overcoming ascending aortic pulsation artifacts that have resulted in both missed and spurious pathologic findings (30,31), ECG synchronization enables assessment of aortic root and coronary ostial involvement. Motion-free images enable reliable identification of the site of the primary intimal tear, location and extent of dissection flaps, and branch-artery involvement—features important in guiding therapy (Figs 2, 3). Visualization of hitherto unknown but common pathologic features (eg, blood pools and side branch communications within an intramural hematoma [IMH] [32]) and the ability to detect subtle lesions previously deemed inaccessible to in vivo diagnostic imaging (ie, limited dissection [30,33]) have allowed CT angiography to lead the way to new classifications of acute aortic lesions (34).

The traditional “classification” of AAS into aortic dissection, IMH, and penetrating atherosclerotic ulcer (PAU) (34,35) can be refined through analysis of CT angiography. Perhaps one of the most important insights gleaned from CT angiography is that in addition to its classic description as a variant of aortic dissection, IMH may be seen in association with virtually any acute aortic abnormality, including the entire spectrum of dissection variants, PAUs, and rupturing aortic aneurysms of any etiology (atherosclerotic, connective tissue-related, mycotic, and even posttraumatic, iatrogenic or noniatrogenic) (Fig 4). Thus, IMH might be more appropriately classified as an imaging marker of acuity associated with aortic dissection, PAU, and rupturing aneurysm rather than the currently in vogue characterization of IMH as a distinct “condition” of AAS (34,35). Moreover, the association of IMH with both the classic AAS conditions of aortic dissection and PAU and with rupturing aortic aneurysm introduces the question as to why rupturing aortic aneurysms are not included as AAS (30).

An alternative concept informed by observations from ECG-gated CT angiography regards AAS as a spectrum of disease manifestations caused by three main pathologic processes: group 1, aortic dissection and its variants resulting from a diseased media; group 2, PAU, which is a manifestation of advanced atherosclerosis and thus a disease of the intima; and group 3, rupturing aortic aneurysms, as the clinical presentation is indistinguishable from aortic dissection and PAU (Table) (30). Note that IMH is not part of this classification as it may be associated with any of the three main categories as an indicator of an acute process.

Group 1 lesions representing aortic dissection and its variants share a diseased aortic media as their common pathologic lesion. *Classic dissection* is characterized by the development of a flow channel or false lumen within the aortic wall, which is separated from the true lumen by a dissection membrane (Fig 2). Blood most commonly flows into the false lumen through a primary intimal tear, and re-enters the true lumen through one or more exit tears.

Regardless of the presence of an identifiable primary intimal tear, when fresh blood coagulates within a false lumen space, we refer to it as an *IMH or dissection variant*. In a small number of patients with medial disease, a superficial/partial thickness tear develops (the equivalent of a primary intimal tear) without the development of a separate flow channel or accumulation of intramural blood. These rare lesions are referred to as *limited tears* or *limited dissection* and tend to have subtle imaging findings when compared with classic dissection (30,33,36) (Fig 3). In patients with medial disease, lesions can evolve rapidly, and features of aortic dissection, IMH, and limited tears can and often do overlap (Fig 5).

Group 2 lesions representing PAUs are characterized by defects in the thickened and diseased intima that penetrate through the internal elastic lamina into deeper layers of the aortic wall, which may be associated with IMH. When associated with PAU, IMH generally has a worse prognosis than uncomplicated IMH associated with medial disease (dissection variant) (37).

Group 3 lesions are rupturing aortic aneurysms, occurring most frequently in the abdominal aorta (Fig 4). Signs of unstable aneurysms are fresh blood within a layer of chronic thrombus (crescent sign), intramural blood, and peri-aneurysmal stranding.

Virtually all structural features associated with AAS and their complications can be reliably assessed with modern CT angiography. The widespread availability of this comprehensive morphologic assessment is providing unique insights into the natural history of AAS, allowing refined classification schemes and better implementation of surgical and endovascular treatments.

Peripheral Vascular Disease: Pushing the Envelope for CT Angiography Coverage and Visualization

CT angiography of the entire lower extremity arterial system—which includes suprainguinal inflow vessels and infrainguinal runoff—became possible with the introduction of multidetector CT (25). While initially limited to 1-minute acquisitions and 2–3-mm-thick sections, modern 64-row CT scanners can achieve 10-second acquisitions with submillimeter section thickness, although such fast scan times are not necessary.

The anatomic coverage for a lower extremity CT angiogram typically extends from T12 through the toes, with a 25–30-cm field of view, to provide adequate in-plane resolution (38). Through-plane resolution (in the z-axis) is typically 0.7–1.25 mm. While lower extremity CT angiography data acquisition is relatively straightforward with state-of-the-art equipment, synchronization with contrast medium delivery requires particular attention to the potentially delayed bolus propagation in a diseased lower extremity arterial tree (39). A simple strategy is to deliberately acquire the CT data in a relatively long scan time of 40 seconds and preprogram an optional second pass from above the knees down through the toes (39).

Together with the advances of multidetector CT, peripheral vascular CT angiography necessitated advances in the capabilities of image processing workstations to accommodate datasets composed of 1000–2000 primary transverse CT reconstructions (40). Because viewing transverse source images is both impractical and inadequate for communicating findings to treating physicians, an important challenge of lower extremity CT angiography is visualization and postprocessing. The classic 3D techniques for displaying cardiovascular CT data, such as maximum intensity projection (MIP) and volume-rendered images are often limited in patients with peripheral artery disease, because approximately half of these patients have significant vessel wall calcifications or stents in place. Both preclude visualization of the diagnostically and therapeutically relevant flow channels (41). Analysis of the vessel lumen is best achieved with curved planar reformation, either through each arterial branch separately (25,42) or as multipath curved planar reformations (43). Processing of lower extremity CT angiography may be time-consuming, and practices with large examination volumes might benefit from using dedicated technologists or a centralized 3D laboratory to generate standardized images of the lower extremity arterial tree.

Lower-extremity CT angiography (and MR angiography) has virtually replaced diagnostic intraarterial angiography for a broad spectrum of indications (38), the most important of which is treatment planning for patients with peripheral artery disease (44). Other indications include acute ischemia, trauma, and anatomic imaging, such as before free-flap harvesting (45), or in athletes suspected of having functional or anatomic popliteal entrapment syndrome (Fig 6), or iliac endofibrosis (38).

The clinical role of lower extremity CT angiography in the setting of peripheral artery disease is not to establish the diagnosis—this is typically based on symptoms, clinical examination, and noninvasive testing such as ankle-brachial index. The strength and role of lower extremity CT angiography is to map the disease process within this large territory, which is critical for treatment planning.

The two main categories of peripheral artery disease warranting intervention are patients with lifestyle-limiting intermittent claudication (Fontaine IIb) and patients with critical limb ischemia (rest-pain and/or tissue loss, Fontaine III and IV) (Fig 7) (46). In the claudication group, treatment aims at symptom relief and is typically restricted to lesions above the knee. In patients with critical limb ischemia, revascularization aims at prevention of tissue loss and amputation, which requires more aggressive endovascular and/or surgical treatment of arteries both above and below the knees.

Lower extremity CT angiography is an accurate imaging modality in patients with intermittent claudication, with a sensitivity of 95% (95% confidence interval: 92%, 97%) and a specificity of 96% (95% confidence interval: 93%, 97%) for detecting more than 50% stenosis or occlusions reported in a recent meta-analysis (47). Similar sensitivities (92%–99.5%) and specificities (64%–99%) have been reported for MR angiography (48). In a randomized controlled trial comparing clinical utility, patient outcomes, and costs between contrast-enhanced MR angiography and CT angiography, no statistically significant differences were found: CT angiography had slightly higher diagnostic confidence and less patients needed additional vascular imaging, with a slight trend of greater clinical

improvement after revascularization based on CT angiography. Average costs for diagnostic imaging was $438 higher in the MR group (95% confidence interval: $255, $632) compared with CT (49). The accuracy of lower extremity CT angiography decreases in below-knee vessels, with the main limiting factor being the presence of arterial calcifications. Since below-knee arteries are not a treatment target in patients with intermittent claudication, this is not a significant drawback in this population (50). However, in patients with critical limb ischemia, who may also be diabetic and may have significant arterial calcification, this a greater concern, and time-resolved MR angiography techniques may be advantageous in this subgroup of patients (51). Recent data suggest, however, that CT angiography provides accurate recommendations for the management of patients with critical limb ischemia as well (52).

Very recently, dual-energy CT technology has become available on commercial CT systems. In principle, basis material decomposition of CT projection data acquired at two different x-ray energy levels (eg, 140 kVp and 80 kVp) allows differentiation of iodine from calcium (53). While successfully applicable to the identification of highly opacified vessels (containing iodine) versus dense calcifications (large plaque or cortical bone) in large proximal vessels, dual-energy CT has not been shown to reliably separate calcium from iodine in small, below-knee peripheral vessels, where this would be particularly desirable (54,55). This may be explained by the low signal intensity provided by low-attenuation contrast medium (due to partial volume artifacts) in small arteries and low-attenuation vessel wall calcium (mostly due to partial volume artifacts related to the limited spatial resolution of current CT systems) in the presence of noise. Continued development of CT technology with improved spatial resolution, better separation of energy spectra, and novel iterative reconstruction and other postprocessing techniques may ultimately overcome the few remaining technical limitations of this powerful technology.

Endovascular Aortic Repair

Wave 1: Aortic Endograft Deployment

Following the first description of endovascular repair of aortic aneurysms using stentgrafts in 1991 (56), the 1990s brought rapid development and commercialization of stent-grafts or “endografts” for the repair of aortic aneurysms (57). Focusing on the most prevalent type of aortic aneurysm, these devices initially were developed to repair infrarenal abdominal aortic aneurysms, but their use was soon expanded to thoracic aortic aneurysms, as well (58).

Prior to the development of aortic stent-grafts, aortic aneurysm repair was exclusively an open surgical procedure. Because the surgical exposure provided the surgeon with direct visualization of the aorta, the demands on imaging to characterize the aorta prior to repair were limited and were focused predominately on identifying the superior and inferior extent of the aneurysm to plan exposure and attribute surgical risk based on the position of the aortic cross-clamp (59). The sizing of the graft was performed intraoperatively by using direct measurement of aortic diameter and fitting of the graft to determine length.

In contrast, stent-graft deployment placed fundamentally new demands on preoperative imaging for qualitative and quantitative analyses. These included determinations of the

suitability of the transarterial delivery route, the proximal fixation and seal zone, and the distal seal zone. The identification and characterization of aortic branches, including main renal, accessory renal, superior and inferior mesenteric, and internal iliac arteries were important to avoid inadvertent end-organ ischemia due to aortic branch occlusion by the stent-graft and to allow for the possibility of predeployment branch embolization to diminish the risk of type II endoleak. Finally, quantitative analysis of the aorta and iliac arteries was necessary to correctly size the device to determine the diameters of the proximal and distal ends and the length of the stent-graft.

While conventional angiography was the standard of the day, its ability to fulfill the demands of predeployment aortic characterization was limited by its inability to demonstrate thrombosed regions of aneurysms and the effects of projection, magnification, and parallax on the accuracy of measurements. Owing to aortic tortuosity and obliquity relative to the longitudinal axis of the CT table, diameter measurements from transverse CT reconstructions were unreliable and associated with substantial interobserver variability (60). Nevertheless transverse measurements of aortic diameter and cranial-caudal dimensions of aortic length were used routinely for stent-graft sizing (61,62). Intravascular ultrasonography (US) became a popular adjunct to conventional angiography and was touted as having greater accuracy than transverse CT reconstructions for determining the diameter and length of stent-grafts (63), but the utility of intra-vascular US for sizing endografts ultimately was refuted (Fig 8) (64).

CT angiography stood apart from the aforementioned imaging modalities as a near-isotropic volumetric acquisition technique that allowed the reformation of Cartesian planar and curved planar (42) images as well as volume renderings (65). The introduction of automated analytical tools to quantify cross-sectional area, length, and arterial curvature or tortuosity offered a process that overcame the many limitations of two-dimensional techniques by allowing measurement of cross-sections that were truly orthogonal to the aortic lumen and allowed measurements to be referenced to both inner and outer wall landmarks (Fig 8) (66). The acceptance of CT angiography as the sole modality of choice for aortic aneurysm characterization and planning of stent-graft deployment was gradual but was firmly established by the end of the early 2000s.

In the early days of aortic endograft procedures, little was known about the natural history of the repair. Owing to the greater complexity of predeployment planning, the limited ability of peri-procedural imaging to assess for robust proximal and distal seals as well as back-bleeding into the aneurysm sac from patent branches and the possibility over time for dislodgment and disintegration of the stent-graft, the necessity for postdeployment surveillance was greater than with conventional repair. In clinical trials of endografts, the combination of conventional angiography and projectional radiography were established as the imaging standard for identifying endoleaks and device displacement, however, CT angiography quickly emerged as a superior modality for endoleak detection (67,68) and ultimately for the detection of stent-graft migration and disintegration, as well (Fig 9) (69). The former observation was based on the elimination of overlapping structures owing to the cross-sectional acquisition and the greater sensitivity of CT for low concentrations of iodine, which for endoleak detection may be subjected to intraarterial dilution prior to entering the

sac via collateral pathways with distant origins (70). Recently published data suggest that MR imaging may be more sensitive than CT angiography for the detection of endoleaks, particularly when used with a blood pool contrast agent (71). While MR imaging may be a useful adjunct to CT in cases in which the aneurysm sac is growing without a demonstrable endoleak on CT images, the versatility of CT angiography to show aortoiliac anatomy as well as the position and integrity of the endograft with or without the use of iodinated contrast material makes it the preferred examination for tracking post-deployment endograft performance (72).

Wave 2: Transcatheter Aortic Valve Implantation

In the 1990s, aortic endografts represented disruptive technology that completely changed the long-established approach to aortic aneurysm repair. Twenty years later, transcatheter aortic valve replacement (TAVR) has emerged as a novel and similarly disruptive technology for repair of the aortic valve in nonoperable and high-risk patients with severe symptomatic aortic stenosis (73,74).

TAVR was first described by means of a transvenous approach by Cribier et al in 2002 (75). Subsequently, an array of alternative transvascular approaches have been developed, including the most common route, the transfemoral arterial approach, but also transaortic, trans-subclavian, and transapical methods, allowing over 60 000 procedures to have been performed worldwide to date. Similar to aortic endograft deployment, the first generation of TAVR development has been largely supported by long-established imaging techniques used for assessing the local anatomy, which for the aortic valve has been echocardiography. This resulted in good but not perfect early results (73,74), leading some to argue that there is no role for CT characterization beyond assessment of the peripheral vascular access route. This sentiment ignores the significant residual complications that remain with TAVR, including paravalvular aortic valvular regurgitation, which is defined by postdeployment transesophageal echocardiography (76) and might be mitigated through a more complete and granular assessment of the annulus.

There is increasing awareness that even a mild degree of paravalvular aortic valvular regurgitation portends a worse prognosis than those patients who experience trace paravalvular aortic valvular regurgitation (77). Moderate to severe paravalvular aortic valvular regurgitation has been observed in 12.9% and 6.8% of TAVR patients at 30 days and 1 year, respectively, compared with 0.9% and 1.8% in the surgical arm of the PARTNER A trial (73,74). While paravalvular aortic valvular regurgitation appears to be multifactorial, with factors such as severity and eccentricity of valvular calcification and malpositioning being important in its etiology, it is widely accepted that undersizing of the transcatheter heart valve relative to the aortic annulus is a significant contributing factor (78).

To understand TAVR, one must first appreciate the noncircular configuration of the annulus. The ovoid geometry is well accepted to be a major cause of paravalvular regurgitation (76) There has been historical underappreciation of this noncircular geometry by two-dimensional transthoracic echocardiographic techniques and it was only well established through the use of ECG-gated CT angiography (79,80). Further, studies using CT

angiography and trans-esophageal echocardiography have established the aortic root as a dynamic structure that undergoes pulsatile contour deformation and configurational change throughout the cardiac cycle related to a number of factors, including the aortic-mitral continuity and the variability of left atrial pressure and volume across the cardiac cycle (81). The isotropic volumetric and time-resolved capabilities of ECG-gated CT angiography provide reproducible and accurate annular measurements throughout the cardiac cycle, providing a reliable means to measure annular area and circumference, which have been shown to be powerful predictors of paravalvular aortic valvular regurgitation (78). Recently transcatheter heart valve stent-sizing algorithms—based on area rather than diameter—have been shown to be more reproducible and have demonstrated more consistent oversizing of the annulus. This technique has been shown to enable a reduction in the burden and severity of paravalvular aortic valvular regurgitation and, when compared with transthoracic echocardiography, reduces extreme over- and undersizing (82). Consequently, CT angiography–derived measurement is becoming the standard for TAVR stent valve selection to optimize annular sizing and ensure controlled oversizing of the aortic annulus (Fig 10), encouraged by the recent reports of significant reductions in paravalvular aortic valvular regurgitation following the integration of CT angiography–based sizing of TAVR stent valves (82,83).

While some investigators have advocated the integration of multidetector CT perimeter-based sizing, there appears to be significant variability in annular circumference measurements across workstation platforms (81). Regardless of the use of perimeter/circumference or area, CT has been consistently shown to provide reproducible and granular assessments of the annulus that are more effective than 3D transesophageal echocardiographic assessments for the identification of patients who are likely to experience greater than mild paravalvular aortic valvular regurgitation. These measurements allow for a more thoughtful and integrated approach to transcatheter heart valve selection than any two-dimensional diameter can provide, enabling more controlled device oversizing and annular stretch. They also provide an opportunity to consider controlled undersizing of self-expanding prostheses or careful balloon underfilling with a balloon expandable valve in the setting of adverse root features such as significant calcification within the left ventricular outflow tract or shallow sinuses of valsalva. While future studies will be needed to determine the optimal method for annular sizing to achieve an effective balance between the minimization of paravalvular aortic valvular regurgitation versus vascular injury, there is no question that over the past 5 years CT has transformed our understanding of annular geometry and has established itself as an essential component of TAVR planning and guidance.

CT Angiography of Coronary Artery Disease: The Final Frontier

Through the 1990s, the rapid evolution of CT technology provided a means for CT angiography applications to develop for virtually every vascular bed. However, one of the most important arterial beds, the coronary arteries, remained elusive. Owing to their position on the surface of the heart, the coronary arteries are in constant motion. Strategies to improve the temporal resolution of CT angiography were needed to “freeze” cardiac motion and allow clear depiction of the coronary arteries and adjacent cardiac structures. While

coronary CT angiography dates back to the mid-1990s using the ECG to prospectively trigger electron-beam CT (84), the limited availability of electron-beam CT prevented the technique from developing beyond a few centers. When multidetector CT was first introduced in 1998 its temporal resolution was substantially worse than the 100-msec resolution of electron-beam CT. Strategies that slowed the CT table to allow retrospective, ECG-gated binning of projections acquired throughout the cardiac cycle substantially broadened the availability of coronary CT angiography (27), however with four-row multidetector CT, retrospective gating was of limited practicality. Within 4 years, 16-row multidetector CT and faster gantry rotations brought substantially greater robustness to coronary CT angiography (85), which has continued to evolve and improve with each iteration of CT technology. Today, coronary CT angiography continues to evolve and establish its role in the diagnostic workup of suspected coronary artery disease (CAD) (Fig 11).

Within the context of patients known to have or suspected of having CAD, anatomic evaluation by means of CT angiography has repeatedly demonstrated overall high performance and an unmatched negative predictive value for noninvasive assessment of CAD (86–88). A meta-analysis of 28 studies, involving 1286 patients, investigating the performance of coronary CT angiography with the now somewhat dated technology of 64-row multidetector CT for the detection of coronary stenosis of 50% or greater, using conventional coronary angiography for a reference standard, reported a per-patient sensitivity of 99%, specificity of 89%, positive predictive value of 93%, and a negative predictive value of 100% (89). Negative predictive value remained 100% on per-vessel analyses. More recently, technical advances have enabled coronary CT angiography to maintain this high level of diagnostic accuracy while drastically reducing the associated radiation exposure through the use of techniques such as prospective ECG-triggering and ECG-gated tube current pulsing. A recent meta-analysis of 14 studies comprising 910 patients who had been investigated with such low-radiation-dose approaches resulted in a sensitivity of 99%, specificity of 91%, positive predictive value of 94%, and negative predictive value of 99% achieved with a modest mean effective radiation dose of 3.3 mSv (90). These techniques have been further refined to provide the necessary information at nominal radiation doses, with the most recent techniques being performed at less than 1 mSv (91).

Within current guidelines for the evaluation of suspected stable angina, CT angiography has been designated appropriate for low-to-intermediate-likelihood patients with prior nondiagnostic or equivocal test results as the most common scenario (92). In contrast to chronic chest pain, the diagnostic algorithm for acute chest pain is much more volatile. Only a small percentage of patients present with sufficiently definitive signs and symptoms to justify direct referral to conventional angiography (93), while a majority of patients are classified as being at intermediate risk, defined as 30%–70% pre-test probability of significant CAD (92). For these patients, additional testing is needed to avoid the expense of prolonged stays in emergency departments or chest pain units. CT angiography appears to be emerging as one of the most efficient and effective methods for reliably ruling out disease (93–95).

Two major multicenter randomized trials involving 1370 and 1000 patients with acute chest pain compared the use of CT angiography to traditional care and found significantly higher direct discharge rates from the emergency department and shorter emergency department stays without an increase in the rate of major adverse cardiac events (93,94).

While the level of evidence in support of the routine clinical use of coronary CT angiography is higher currently than for any other application of CT angiography and the number of patients who present with suspected CAD dwarfs that of all other CT angiography indications, heightened concerns over the cost of widespread CT angiography utilization in the evaluation of patients with chest pain has resulted in highly heterogeneous reimbursement and thus utilization of coronary CT angiography in the United States. This remains 5 years after two analyses of patients at low and intermediate risk of major adverse cardiac events, respectively, demonstrated a 26%–33% reduction in CAD-related costs without an increase in adverse cardiovascular events or CAD-related hospitalization, following initial evaluation at CT angiography when compared with initial evaluation at single photon emission computed tomography (SPECT), the traditional modality for first-line cardiac function assessment (95,96).

One important concern regarding the performance of coronary CT angiography is that its positive predictive value is not nearly as robust as its negative predictive value. Given the high prevalence of clinical symptoms where CAD is within the differential diagnosis, there remain concerns that false-positive results from the routine use of coronary CT angiography will increase downstream costs. Two strategies are emerging that could substantially improve the positive predicative value of coronary CT angiography by associating functional information with the standard morphologic assessment—CT imaging of myocardial perfusion and CT-derived fractional flow reserve (FFR_{CT}) measurements. The former technique has been enabled through ongoing advances in CT technology, while the latter technique relies on sophisticated postprocessing and analysis of coronary CT angiographic data.

Myocardial Perfusion

In current clinical practice, the hemodynamic relevance of coronary lesions has been derived from measures of myocardial perfusion by using SPECT, positron emission tomography (PET), and more recently, cardiac perfusion MR imaging, offering a means for risk stratification, guidance for treatment strategy, and outcome prediction (97).

Initial CT-derived insights into the myocardial blood supply have been derived from diagnostic, “static” coronary CT angiographic examinations. Myocardial attenuation patterns are used to assess myocardial blood volume qualitatively, as a surrogate for myocardial perfusion during the first-pass arterial phase. Hypoattenuating territories accompanied by stenoses within associated coronaries are indicative of hemodynamically significant CAD (98). However, important limitations of this approach to approximate myocardial perfusion measurements include the variability of normal myocardial enhancement during image acquisition and an inability to quantify the results.

Two recent advances in CT technology are enabling more robust CT-based measurement of myocardial perfusion. Discussed previously within the context of minimizing the impact of mural calcium on the assessment of the lower extremity arterial runoff, dual-energy CT has the potential to resolve iodine concentration within the myocardium (99). This method can improve the CT assessment of myocardial blood supply yielding results that are comparable to MR imaging and SPECT perfusion imaging (100) but augmented substantially by the associated anatomic information. Dual-energy CT has also been shown to allow for improvements in image quality and reduction in artifacts such as beam hardening that have traditionally limited CT perfusion imaging (101). While dual-energy technology appears to improve myocardial assessment, when used as a part of a uniphasic acquisition during the first arterial pass through the myocardium, its capabilities for quantification are limited (98).

This latter concern may be eliminated through the second advance that provides wide area detectors and the ability to rapidly shuttle across the imaging volume during the transit of contrast material through the myocardium, thus enabling dynamic CT myocardial perfusion imaging (Fig 12). Dynamic iodine-based CT perfusion can provide an absolute quantitative measure of myocardial blood flow, an advantage over MR imaging, which suffers from a nonlinearity in the relationship between myocardial signal and gadolinium concentration (102). Investigations of dynamic CT measurements of perfusion support a threshold of 75–90 $mL \cdot 100\ mL^{-1} \cdot min^{-1}$, below which coronary lesions should be considered hemodynamically significant (103–105). One concern related to the use of dynamic CT measurements of perfusion is the increased radiation dose associated with the extended acquisition; however, the radiation doses are reported to be similar to that of SPECT perfusion imaging (105), the traditional method for obtaining such information. Moreover, as will be discussed subsequently, advancements in iterative reconstruction methods for CT should result in further reductions in radiation exposure.

While efforts at deriving measures of myocardial perfusion with CT are currently in a state of relative infancy, the appeal of obtaining comprehensive anatomic and functional assessments in the workup of ischemic heart disease with a single instrumental set-up is strong. At the time of this writing, clinical performance data are pending from a multitude of ongoing single- and multicenter trials to establish the role of CT perfusion in the diagnostic algorithm of CAD.

Estimating Lesion-Specific Ischemia from Resting CT Angiography

Historical management of stable angina has been focused on the revascularization of anatomic stenosis with an angiographic measure of diameter reduction being the guide. Recent data has suggested that revascularization guided by lesion-specific ischemia as determined by invasively measured fractional flow reserve (FFR) improves event-free survival over decisions based on angiography alone (106). Coronary arterial FFR is measured as the ratio of the systolic blood pressure distal to a coronary artery stenosis divided by the systolic blood pressure in the ascending aorta during pharmacologically induced flow maximization. It has also been well established that visual inspection and even quantitative assessment of diameter reduction with either conventional or coronary CT angiography provide limited information regarding lesion specific ischemia (106,107).

Advances in computational fluid dynamics and image-based modeling as well as continued improvement in image quality of coronary CT angiography has allowed the calculation of coronary flow and pressure from a typically acquired routine resting coronary CT angiogram (108,109) allowing the calculation of an FFR without the modification of imaging protocols, additional imaging, increase in radiation exposure, or the addition of pharmacologic stress agents. Coronary artery flow and pressure can be derived by using the governing (Navier-Stokes) equations of fluid dynamics, but until recently there has not been the computational power or an adequate noninvasive model of the coronary arteries to apply them to derive a noninvasive FFR. More complete methods describing in detail the basis for FFR_{CT} derivation are beyond the scope of this review and have been described in detail elsewhere (110).

While only a recent development, there is increasing evidence for the high diagnostic performance of FFR_{CT} for the determination of lesion-specific ischemia, with invasive FFR as the reference standard (Fig 13). Of importance, all published data until now have shown the superiority of FFR_{CT} as compared with coronary CT angiography alone.

A prospective, multicenter international trial found that FFR_{CT} surpassed CT angiography as a predictor of ischemia across all measures of diagnostic performance (108). FFR_{CT} displayed significantly higher discriminatory ability than CT angiography for lesion-specific ischemia (area under the curve: 0.90 for FFR_{CT} vs 0.75 for coronary CT angiography, $P = .001$). The investigators also found that traditional anatomic stenosis characterization at CT angiography added little to FFR_{CT}. Moreover, for the distinctly clinically challenging 58% of patients with at least one 40%–69% stenosis by means of quantitative coronary angiography, 47% of the lesions were associated with ischemia by means of FFR. For these intermediate stenoses, FFR_{CT} demonstrated a diagnostic accuracy, sensitivity, specificity, positive predictive value, and negative predictive value of 86%, 90%, 83%, 82%, and 91%, respectively, compared with 56%, 90%, 26%, 52%, and 75% for the same measures derived by means of standard CT angiographic interpretation (111).

More recently, a larger trial confirmed that on a per-patient analysis, FFR_{CT} is superior to traditional CT angiography analysis for predicting ischemia in stenoses of 50% or greater, showing significantly better lesion discrimination when compared with CT stenosis of 50% or greater (AUC: 0.81 versus 0.68, $P = .0002$) (109). When a decision rule was applied wherein only vessels 2 mm or greater in size were included in the analysis and all vessels with less than 30% stenosis were considered nonischemic, the performance of FFR_{CT} was extremely robust, with an accuracy of 92% for FFR_{CT} versus 68% for CT angiography–based stenosis characterization alone ($P < .0001$) (109).

While last among major applications to enter into the clinical realm, a combination of remarkable technologic developments by CT manufacturers, advances in image processing and analysis, and dedication and creativity of investigators from the fields of radiology and cardiology has enabled CT angiography of CAD to undergo the most profound transformation of any CT angiography application. Based on the knowledge gained to date and the trajectory of further innovation, coronary CT angiography appears poised to play a major role in the diagnosis and management of CAD in the near future.

Concerns for Radiation

Concerns have been advanced in the lay press and the professional literature regarding potential risks arising from the growth in CT utilization. These concerns have focused on radiation exposure principally (112), particularly in children (113). Nevertheless, large uncertainties remain regarding the stochastic risk of cancer induction from radiation at medical imaging. According to current evidence, across an adult population, risks of medical imaging at effective doses below 50 mSv for single procedures or 100 mSv for multiple procedures over short time periods are likely too low to be epidemiologically detectable and may be nonexistent (114). However, because of these uncertainties, imagers must always remain vigilant to assure that medical imaging procedures are performed for appropriate indications and conducted at the lowest radiation dose that delineates the necessary clinical information so that the risks of imaging do not exceed their benefits and scans are performed with the lowest dose allowable (115). The realization of these principles is aided by recent advances in CT technology, particularly the reintroduction and refinement of iterative reconstruction as a substitute for filtered back projection (116), which have reduced the radiation exposure associated with CT angiography substantially and should continue to do so as further refinements evolve (117).

Summary

Over a short 20-year span, CT angiography has evolved from a fledgling imaging modality, incapable of encompassing most vascular territories, to a critical clinical tool that plays a dominant role in the diagnosis and management of disease within virtually every arterial bed in the body. While technological developments in CT acquisition and image processing techniques have enabled great innovation and important discovery, there is no sign of this trend slowing. Indeed the evolution of novel CT scanner geometries, alternative raw data reconstruction strategies, and sophisticated postprocessing techniques are paving the way for the further evolution of CT angiography to provide greater relevance in predicting the clinical importance of cardiovascular lesions and facilitating their effective management.

Abbreviations

AAS	acute aortic syndrome
CAD	coronary artery disease
ECG	electrocardiography
FFR	fractional flow reserve
FFR_{CT}	CT-derived fractional flow reserve
IMH	intramural hematoma
MIP	maximum intensity projection
PAU	penetrating atherosclerotic ulcer
TAVR	transcatheter aortic valve replacement

3D three dimensional

References

1. Brooks B. Intra-arterial injection of sodium iodid: preliminary report. JAMA. 1924; 82(13):1016–1019.
2. Seldinger SI. Catheter replacement of the needle in percutaneous arteriography: a new technique. Acta Radiol. 1953; 39(5 Suppl):368–376. [PubMed: 13057644]
3. Dumoulin CL, Hart HR Jr. Magnetic resonance angiography in the head and neck. Acta Radiol Suppl. 1986; 369:17–20. [PubMed: 2980442]
4. Nishimura DG, Macovski A, Pauly JM. Magnetic resonance angiography. IEEE Trans Med Imaging. 1986; 5(3):140–151. [PubMed: 18244000]
5. Wing VW, Federle MP, Morris JA Jr, Jeffrey RB, Bluth R. The clinical impact of CT for blunt abdominal trauma. AJR Am J Roentgenol. 1985; 145(6):1191–1194. [PubMed: 3877421]
6. Kalender WA, Seissler W, Klotz E, Vock P. Spiral volumetric CT with single-breath-hold technique, continuous transport, and continuous scanner rotation. Radiology. 1990; 176(1):181–183. [PubMed: 2353088]
7. Crawford CR, King KF. Computed tomography scanning with simultaneous patient translation. Med Phys. 1990; 17(6):967–982. [PubMed: 2280740]
8. Rubin GD, Shiau MC, Schmidt AJ, et al. Computed tomographic angiography: historical perspective and new state-of-the-art using multi detector-row helical computed tomography. J Comput Assist Tomogr. 1999; 23(Suppl 1):S83–S90. [PubMed: 10608402]
9. Napel S, Marks MP, Rubin GD, et al. CT angiography with spiral CT and maximum intensity projection. Radiology. 1992; 185(2):607–610. [PubMed: 1410382]
10. Schwartz RB, Jones KM, Chernoff DM, et al. Common carotid artery bifurcation: evaluation with spiral CT. Work in progress. Radiology. 1992; 185(2):513–519. [PubMed: 1410365]
11. Vieco PT, Shuman WP, Alsofrom GF, Gross CE. Detection of circle of Willis aneurysms in patients with acute sub-arachnoid hemorrhage: a comparison of CT angiography and digital subtraction angiography. AJR Am J Roentgenol. 1995; 165(2):425–430. [PubMed: 7618571]
12. Galanski M, Prokop M, Chavan A, Schaefer CM, Jandeleit K, Nischelsky JE. Renal arterial stenoses: spiral CT angiography. Radiology. 1993; 189(1):185–192. [PubMed: 8372191]
13. Rubin GD, Dake MD, Napel SA, McDonnell CH, Jeffrey RB Jr. Three-dimensional spiral CT angiography of the abdomen: initial clinical experience. Radiology. 1993; 186(1):147–152. [PubMed: 8416556]
14. Remy-Jardin M, Remy J, Wattinne L, Giraud F. Central pulmonary thromboembolism: diagnosis with spiral volumetric CT with the single-breath-hold technique—comparison with pulmonary angiography. Radiology. 1992; 185(2):381–387. [PubMed: 1410342]
15. Costello P, Ecker CP, Tello R, Hartnell GG. Assessment of the thoracic aorta by spiral CT. AJR Am J Roentgenol. 1992; 158(5):1127–1130. [PubMed: 1566679]
16. Polacin A, Kalender WA, Marchal G. Evaluation of section sensitivity profiles and image noise in spiral CT. Radiology. 1992; 185(1):29–35. [PubMed: 1523331]
17. Remy J, Remy-Jardin M, Wattinne L, Deffontaines C. Pulmonary arteriovenous malformations: evaluation with CT of the chest before and after treatment. Radiology. 1992; 182(3):809–816. [PubMed: 1535899]
18. Schwickert HC, Schweden F, Schild HH, Renner C, Iverson PD. Chronic thromboembolic pulmonary artery obstruction: CT diagnosis and follow-up after thrombend-arterectomy [abstr]. Radiology. 1993; 189(P):153. [PubMed: 7690489]
19. Rubin GD, Dake MD, Napel S, et al. Spiral CT of renal artery stenosis: comparison of three-dimensional rendering techniques. Radiology. 1994; 190(1):181–189. [PubMed: 8259402]
20. Gavant ML, Menke PG, Fabian T, Flick PA, Graney MJ, Gold RE. Blunt traumatic aortic rupture: detection with helical CT of the chest. Radiology. 1995; 197(1):125–133. [PubMed: 7568809]

21. Rubin GD, Alfrey EJ, Dake MD, et al. Assessment of living renal donors with spiral CT. Radiology. 1995; 195(2):457–462. [PubMed: 7724766]
22. Van Hoe L, Baert AL, Gryspeerdt S, et al. Supra- and juxtarenal aneurysms of the abdominal aorta: preoperative assessment with thin-section spiral CT. Radiology. 1996; 198(2):443–448. [PubMed: 8596847]
23. Rubin GD, Shiau MC, Leung AN, Kee ST, Logan LJ, Sofilos MC. Aorta and iliac arteries: single versus multiple detector-row helical CT angiography. Radiology. 2000; 215(3):670–676. [PubMed: 10831682]
24. Fleischmann, D. Contrast medium administration in computed tomographic angiography. In: Rubin, GD.; Rofsky, NM., editors. CT and MR angiography: comprehensive vascular assessment. Philadelphia, Pa: Lippincott Williams & Wilkins; 2009. p. 129-154.
25. Rubin GD, Schmidt AJ, Logan LJ, et al. Multidetector-row CT angiography of lower extremity occlusive disease: a new application for CT scanning [abstr]. Radiology. 1999; 210(P):588.
26. Bogdan MA, Klein MB, Rubin GD, McAdams TR, Chang J. CT angiography in complex upper extremity reconstruction. J Hand Surg [Br]. 2004; 29(5):465–469.
27. Achenbach S, Ulzheimer S, Baum U, et al. Noninvasive coronary angiography by retrospectively ECG-gated multislice spiral CT. Circulation. 2000; 102(23):2823–2828. [PubMed: 11104739]
28. Vilacosta I, Román JAS. Acute aortic syndrome. Heart. 2001; 85(4):365–368. [PubMed: 11250953]
29. Hayter RG, Rhea JT, Small A, Tafazoli FS, Novelline RA. Suspected aortic dissection and other aortic disorders: multi-detector row CT in 373 cases in the emergency setting. Radiology. 2006; 238(3):841–852. [PubMed: 16452396]
30. Fleischmann D, Mitchell RS, Miller DC. Acute aortic syndromes: new insights from electrocardiographically gated computed tomography. Semin Thorac Cardiovasc Surg. 2008; 20(4):340–347. [PubMed: 19251175]
31. Chin AS, Fleischmann D. State-of-the-art computed tomography angiography of acute aortic syndrome. Semin Ultrasound CT MR. 2012; 33(3):222–234. [PubMed: 22624967]
32. Williams DM, Cronin P, Dasika N, et al. Aortic branch artery pseudoaneurysms accompanying aortic dissection. Part II. Distinction from penetrating atherosclerotic ulcers. J Vasc Interv Radiol. 2006; 17(5):773–781. [PubMed: 16687742]
33. Svensson LG, Labib SB, Eisenhauer AC, Butterly JR. Intimal tear without hematoma: an important variant of aortic dissection that can elude current imaging techniques. Circulation. 1999; 99(10): 1331–1336. [PubMed: 10077517]
34. Hiratzka LF, Bakris GL, Beckman JA, et al. 2010 ACCF/AHA/AATS/ACR/ASA/SCA/SCAI/SIR/STS/SVM guidelines for the diagnosis and management of patients with Thoracic Aortic Disease: a report of the American College of Cardiology Foundation/American Heart Association Task Force on Practice Guidelines, American Association for Thoracic Surgery, American College of Radiology, American Stroke Association, Society of Cardiovascular Anesthesiologists, Society for Cardiovascular Angiography and Interventions, Society of Interventional Radiology, Society of Thoracic Surgeons, and Society for Vascular Medicine. Circulation. 2010; 121(13):e266–e369. [PubMed: 20233780]
35. Evangelista A, Mukherjee D, Mehta RH, et al. Acute intramural hematoma of the aorta: a mystery in evolution. Circulation. 2005; 111(8):1063–1070. [PubMed: 15710757]
36. Chirillo F, Salvador L, Bacchion F, Grisolia EF, Valfrè C, Olivari Z. Clinical and anatomical characteristics of subtle-discrete dissection of the ascending aorta. Am J Cardiol. 2007; 100(8): 1314–1319. [PubMed: 17920378]
37. Demers P, Miller DC, Mitchell RS, Kee ST, Chagonjian L, Dake MD. Stent-graft repair of penetrating atherosclerotic ulcers in the descending thoracic aorta: mid-term results. Ann Thorac Surg. 2004; 77(1):81–86. [PubMed: 14726040]
38. Fleischmann D, Hallett RL, Rubin GD. CT angiography of peripheral arterial disease. J Vasc Interv Radiol. 2006; 17(1):3–26. [PubMed: 16415129]
39. Fleischmann D, Rubin GD. Quantification of intravenously administered contrast medium transit through the peripheral arteries: implications for CT angiography. Radiology. 2005; 236(3):1076–1082. [PubMed: 16000649]

40. Rubin GD. Data explosion: the challenge of multidetector-row CT. Eur J Radiol. 2000; 36(2):74–80. [PubMed: 11116170]
41. Ouwendijk R, Kock MC, van Dijk LC, van Sambeek MR, Stijnen T, Hunink MG. Vessel wall calcifications at multi-detector row CT angiography in patients with peripheral arterial disease: effect on clinical utility and clinical predictors. Radiology. 2006; 241(2):603–608. [PubMed: 16966479]
42. Raman R, Napel S, Beaulieu CF, Bain ES, Jeffrey RB Jr, Rubin GD. Automated generation of curved planar reformations from volume data: method and evaluation. Radiology. 2002; 223(1): 275–280. [PubMed: 11930078]
43. Roos JE, Fleischmann D, Koechl A, et al. Multipath curved planar reformation of the peripheral arterial tree in CT angiography. Radiology. 2007; 244(1):281–290. [PubMed: 17495179]
44. Schernthaner R, Stadler A, Lomoschitz F, et al. Multidetector CT angiography in the assessment of peripheral arterial occlusive disease: accuracy in detecting the severity, number, and length of stenoses. Eur Radiol. 2008; 18(4):665–671. [PubMed: 18094974]
45. Chow LC, Napoli A, Klein MB, Chang J, Rubin GD. Vascular mapping of the leg with multi-detector row CT angiography prior to free-flap transplantation. Radiology. 2005; 237(1):353–360. [PubMed: 16100083]
46. Norgren L, Hiatt WR, Dormandy JA, et al. Inter-Society Consensus for the Management of Peripheral Arterial Disease (TASC II). J Vasc Surg. 2007; 45(Suppl S):S5–S67. [PubMed: 17223489]
47. Met R, Bipat S, Legemate DA, Reekers JA, Koelemay MJ. Diagnostic performance of computed tomography angiography in peripheral arterial disease: a systematic review and meta-analysis. JAMA. 2009; 301(4):415–424. [PubMed: 19176443]
48. Collins R, Cranny G, Burch J, et al. A systematic review of duplex ultrasound, magnetic resonance angiography and computed tomography angiography for the diagnosis and assessment of symptomatic, lower limb peripheral arterial disease. Health Technol Assess. 2007; 11(20):iii–iv. xi–xiii, 1–184.
49. Ouwendijk R, de Vries M, Pattynama PM, et al. Imaging peripheral arterial disease: a randomized controlled trial comparing contrast-enhanced MR angiography and multi-detector row CT angiography. Radiology. 2005; 236(3):1094–1103. [PubMed: 16020559]
50. Schernthaner R, Fleischmann D, Lomoschitz F, Stadler A, Lammer J, Loewe C. Effect of MDCT angiographic findings on the management of intermittent claudication. AJR Am J Roentgenol. 2007; 189(5):1215–1222. [PubMed: 17954664]
51. Pollak AW, Norton PT, Kramer CM. Multimodality imaging of lower extremity peripheral arterial disease: current role and future directions. Circ Cardiovasc Imaging. 2012; 5(6):797–807. [PubMed: 23169982]
52. Schernthaner R, Fleischmann D, Stadler A, Schernthaner M, Lammer J, Loewe C. Value of MDCT angiography in developing treatment strategies for critical limb ischemia. AJR Am J Roentgenol. 2009; 192(5):1416–1424. [PubMed: 19380571]
53. Alvarez RE, Macovski A. Energy-selective reconstructions in X-ray computerized tomography. Phys Med Biol. 1976; 21(5):733–744. [PubMed: 967922]
54. Tran DN, Straka M, Roos JE, Napel S, Fleischmann D. Dual-energy CT discrimination of iodine and calcium: experimental results and implications for lower extremity CT angiography. Acad Radiol. 2009; 16(2):160–171. [PubMed: 19124101]
55. Kau T, Eicher W, Reiterer C, et al. Dual-energy CT angiography in peripheral arterial occlusive disease-accuracy of maximum intensity projections in clinical routine and subgroup analysis. Eur Radiol. 2011; 21(8):1677–1686. [PubMed: 21365195]
56. Parodi JC, Palmaz JC, Barone HD. Trans-femoral intraluminal graft implantation for abdominal aortic aneurysms. Ann Vasc Surg. 1991; 5(6):491–499. [PubMed: 1837729]
57. Moore WS, Vescera CL. Repair of abdominal aortic aneurysm by transfemoral endovascular graft placement. Ann Surg. 1994; 220(3):331–339. discussion 339–341. [PubMed: 8092899]
58. Dake MD, Miller DC, Semba CP, Mitchell RS, Walker PJ, Liddell RP. Transluminal placement of endovascular stent-grafts for the treatment of descending thoracic aortic aneurysms. N Engl J Med. 1994; 331(26):1729–1734. [PubMed: 7984192]

59. Landry G, Lau I, Liem T, Mitchell E, Moneta G. Open abdominal aortic aneurysm repair in the endovascular era: effect of clamp site on outcomes. Arch Surg. 2009; 144(9):811–816. [PubMed: 19797104]
60. Jaakkola P, Hippeläinen M, Farin P, Rytkönen H, Kainulainen S, Partanen K. Interobserver variability in measuring the dimensions of the abdominal aorta: comparison of ultrasound and computed tomography. Eur J Vasc Endovasc Surg. 1996; 12(2):230–237. [PubMed: 8760988]
61. Moritz JD, Rotermund S, Keating DP, Oestmann JW. Infrarenal abdominal aortic aneurysms: implications of CT evaluation of size and configuration for placement of endovascular aortic grafts. Radiology. 1996; 198(2):463–466. [PubMed: 8596850]
62. Beebe HG, Jackson T, Pigott JP. Aortic aneurysm morphology for planning endovascular aortic grafts: limitations of conventional imaging methods. J Endovasc Surg. 1995; 2(2):139–148. [PubMed: 9234126]
63. White RA, Donayre C, Kopchok G, Walot I, Wilson E, de Virgilio C. Intravascular ultrasound: the ultimate tool for abdominal aortic aneurysm assessment and endovascular graft delivery. J Endovasc Surg. 1997; 4(1):45–55. [PubMed: 9034919]
64. Tillich M, Hill BB, Paik DS, et al. Prediction of aortoiliac stent-graft length: comparison of measurement methods. Radiology. 2001; 220(2):475–483. [PubMed: 11477256]
65. Fishman EK, Drebin B, Magid D, et al. Volumetric rendering techniques: applications for three-dimensional imaging of the hip. Radiology. 1987; 163(3):737–738. [PubMed: 3575725]
66. Rubin GD, Paik DS, Johnston PC, Napel S. Measurement of the aorta and its branches with helical CT. Radiology. 1998; 206(3):823–829. [PubMed: 9494508]
67. Rozenblit A, Marin ML, Veith FJ, Cynamon J, Wahl SI, Bakal CW. Endovascular repair of abdominal aortic aneurysm: value of postoperative follow-up with helical CT. AJR Am J Roentgenol. 1995; 165(6):1473–1479. [PubMed: 7484590]
68. Armerding MD, Rubin GD, Beaulieu CF, et al. Aortic aneurysmal disease: assessment of stent-graft treatment-CT versus conventional angiography. Radiology. 2000; 215(1):138–146. [PubMed: 10751479]
69. Roos JE, Hellinger JC, Hallet R, Fleischmann D, Zarins CK, Rubin GD. Detection of endograft fractures with multidetector row computed tomography. J Vasc Surg. 2005; 42(5):1002–1006. [PubMed: 16275461]
70. Golzarian J, Dussaussois L, Abada HT, et al. Helical CT of aorta after endoluminal stent-graft therapy: value of biphasic acquisition. AJR Am J Roentgenol. 1998; 171(2):329–331. [PubMed: 9694445]
71. Cornelissen SA, Prokop M, Verhagen HJ, Adriaensen ME, Moll FL, Bartels LW. Detection of occult endoleaks after endovascular treatment of abdominal aortic aneurysm using magnetic resonance imaging with a blood pool contrast agent: preliminary observations. Invest Radiol. 2010; 45(9):548–553. [PubMed: 20644485]
72. Bley TA, Chase PJ, Reeder SB, et al. Endovascular abdominal aortic aneurysm repair: nonenhanced volumetric CT for follow-up. Radiology. 2009; 253(1):253–262. [PubMed: 19703867]
73. Leon MB, Smith CR, Mack M, et al. Transcatheter aortic-valve implantation for aortic stenosis in patients who cannot undergo surgery. N Engl J Med. 2010; 363(17):1597–1607. [PubMed: 20961243]
74. Smith CR, Leon MB, Mack MJ, et al. Transcatheter versus surgical aortic-valve replacement in high-risk patients. N Engl J Med. 2011; 364(23):2187–2198. [PubMed: 21639811]
75. Cribier A, Eltchaninoff H, Bash A, et al. Percutaneous transcatheter implantation of an aortic valve prosthesis for calcific aortic stenosis: first human case description. Circulation. 2002; 106(24): 3006–3008. [PubMed: 12473543]
76. Leon MB, Piazza N, Nikolsky E, et al. Standardized endpoint definitions for Transcatheter Aortic Valve Implantation clinical trials: a consensus report from the Valve Academic Research Consortium. J Am Coll Cardiol. 2011; 57(3):253–269. [PubMed: 21216553]
77. Kodali SK, Williams MR, Smith CR, et al. Two-year outcomes after transcatheter or surgical aortic-valve replacement. N Engl J Med. 2012; 366(18):1686–1695. [PubMed: 22443479]

78. Willson AB, Webb JG, Labounty TM, et al. 3-dimensional aortic annular assessment by multidetector computed tomography predicts moderate or severe paravalvular regurgitation after transcatheter aortic valve replacement: a multicenter retrospective analysis. J Am Coll Cardiol. 2012; 59(14):1287–1294. [PubMed: 22365423]

79. Leipsic J, Gurvitch R, Labounty TM, et al. Multidetector computed tomography in transcatheter aortic valve implantation. JACC Cardiovasc Imaging. 2011; 4(4):416–429. [PubMed: 21492818]

80. Blanke P, Schoepf UJ, Leipsic JA. CT in transcatheter aortic valve replacement. Radiology. 2013; 269(3):650–669. [PubMed: 24261496]

81. Hamdan A, Guetta V, Konen E, et al. Deformation dynamics and mechanical properties of the aortic annulus by 4-dimensional computed tomography: insights into the functional anatomy of the aortic valve complex and implications for transcatheter aortic valve therapy. J Am Coll Cardiol. 2012; 59(2):119–127. [PubMed: 22222074]

82. Binder RK, Webb JG, Willson AB, et al. The impact of integration of a multidetector computed tomography annulus area sizing algorithm on outcomes of transcatheter aortic valve replacement: a prospective, multicenter, controlled trial. J Am Coll Cardiol. 2013; 62(5):431–438. [PubMed: 23684679]

83. Jilaihawi H, Kashif M, Fontana G, et al. Cross-sectional computed tomographic assessment improves accuracy of aortic annular sizing for transcatheter aortic valve replacement and reduces the incidence of paravalvular aortic regurgitation. J Am Coll Cardiol. 2012; 59(14):1275–1286. [PubMed: 22365424]

84. Achenbach S, Moshage W, Bachmann K. Detection of high-grade restenosis after PTCA using contrast-enhanced electron beam CT. Circulation. 1997; 96(9):2785–2788. [PubMed: 9386138]

85. Garcia MJ, Lessick J, Hoffmann MH. CATSCAN Study Investigators. Accuracy of 16-row multidetector computed tomography for the assessment of coronary artery stenosis. JAMA. 2006; 296(4):403–411. [PubMed: 16868298]

86. Budoff MJ, Dowe D, Jollis JG, et al. Diagnostic performance of 64-multidetector row coronary computed tomographic angiography for evaluation of coronary artery stenosis in individuals without known coronary artery disease: results from the prospective multicenter ACCURACY (Assessment by Coronary Computed Tomographic Angiography of Individuals Undergoing Invasive Coronary Angiography) trial. J Am Coll Cardiol. 2008; 52(21):1724–1732. [PubMed: 19007693]

87. Miller JM, Rochitte CE, Dewey M, et al. Diagnostic performance of coronary angiography by 64-row CT. N Engl J Med. 2008; 359(22):2324–2336. [PubMed: 19038879]

88. Meijboom WB, Meijs MF, Schuijf JD, et al. Diagnostic accuracy of 64-slice computed tomography coronary angiography: a prospective, multicenter, multivendor study. J Am Coll Cardiol. 2008; 52(25):2135–2144. [PubMed: 19095130]

89. Mowatt G, Cook JA, Hillis GS, et al. 64-Slice computed tomography angiography in the diagnosis and assessment of coronary artery disease: systematic review and meta-analysis. Heart. 2008; 94(11):1386–1393. [PubMed: 18669550]

90. Sun Z, Ng KH. Diagnostic value of coronary CT angiography with prospective ECG-gating in the diagnosis of coronary artery disease: a systematic review and meta-analysis. Int J Cardiovasc Imaging. 2012; 28(8):2109–2119. [PubMed: 22212661]

91. Achenbach S, Marwan M, Ropers D, et al. Coronary computed tomography angiography with a consistent dose below 1 mSv using prospectively electrocardiogram-triggered high-pitch spiral acquisition. Eur Heart J. 2010; 31(3):340–346. [PubMed: 19897497]

92. Taylor AJ, Cerqueira M, Hodgson JM, et al. ACCF/SCCT/ACR/AHA/ASE/ASNC/ NASCI/SCAI/ SCMR 2010 Appropriate Use Criteria for Cardiac Computed Tomography. A Report of the American College of Cardiology Foundation Appropriate Use Criteria Task Force, the Society of Cardiovascular Computed Tomography, the American College of Radiology, the American Heart Association, the American Society of Echocardiography, the American Society of Nuclear Cardiology, the North American Society for Cardiovascular Imaging, the Society for Cardiovascular Angiography and Interventions, and the Society for Cardiovascular Magnetic Resonance. Circulation. 2010; 122(21):e525–e555. [PubMed: 20975004]

93. Litt HI, Gatsonis C, Snyder B, et al. CT angiography for safe discharge of patients with possible acute coronary syndromes. N Engl J Med. 2012; 366(15):1393–1403. [PubMed: 22449295]

94. Hoffmann U, Truong QA, Schoenfeld DA, et al. Coronary CT angiography versus standard evaluation in acute chest pain. N Engl J Med. 2012; 367(4):299–308. [PubMed: 22830462]

95. Min JK, Kang N, Shaw LJ, et al. Costs and clinical outcomes after coronary multidetector CT angiography in patients without known coronary artery disease: comparison to myocardial perfusion SPECT. Radiology. 2008; 249(1):62–70. [PubMed: 18796668]

96. Min JK, Shaw LJ, Berman DS, Gilmore A, Kang N. Costs and clinical outcomes in individuals without known coronary artery disease undergoing coronary computed to-mographic angiography from an analysis of Medicare category III transaction codes. Am J Cardiol. 2008; 102(6):672–678. [PubMed: 18773986]

97. Schwitter J, Wacker CM, Wilke N, et al. MR-IMPACT II: Magnetic Resonance Imaging for Myocardial Perfusion Assessment in Coronary artery disease Trial: perfusion-cardiac magnetic resonance vs. single-photon emission computed tomography for the detection of coronary artery disease: a comparative multicentre, multivendor trial. Eur Heart J. 2013; 34(10):775–781. [PubMed: 22390914]

98. Vliegenthart R, Henzler T, Moscariello A, et al. CT of coronary heart disease: Part 1, CT of myocardial infarction, ischemia, and viability. AJR Am J Roentgenol. 2012; 198(3):531–547. [PubMed: 22357992]

99. Ruzsics B, Lee H, Powers ER, Flohr TG, Costello P, Schoepf UJ. Images in cardiovascular medicine. Myocardial ischemia diagnosed by dual-energy computed tomography: correlation with single-photon emission computed tomography. Circulation. 2008; 117(9):1244–1245. [PubMed: 18316501]

100. Arnoldi E, Lee YS, Ruzsics B, et al. CT detection of myocardial blood volume deficits: dual-energy CT compared with single-energy CT spectra. J Cardiovasc Comput Tomogr. 2011; 5(6): 421–429. [PubMed: 22146501]

101. Scheske JA, O'Brien JM, Earls JP, et al. Coronary artery imaging with single-source rapid kilovolt peak-switching dual-energy CT. Radiology. 2013; 268(3):702–709. [PubMed: 23579045]

102. Gerber BL, Belge B, Legros GJ, et al. Characterization of acute and chronic myocardial infarcts by multidetector computed tomography: comparison with contrast-enhanced magnetic resonance. Circulation. 2006; 113(6):823–833. [PubMed: 16461822]

103. Gerber TC, Carr JJ, Arai AE, et al. Ionizing radiation in cardiac imaging: a science advisory from the American Heart Association Committee on Cardiac Imaging of the Council on Clinical Cardiology and Committee on Cardiovascular Imaging and Intervention of the Council on Cardiovascular Radiology and Intervention. Circulation. 2009; 119(7):1056–1065. [PubMed: 19188512]

104. Bamberg F, Becker A, Schwarz F, et al. Detection of hemodynamically significant coronary artery stenosis: incremental diagnostic value of dynamic CT-based myocardial perfusion imaging. Radiology. 2011; 260(3):689–698. [PubMed: 21846761]

105. Wang Y, Qin L, Shi X, et al. Adenosine-stress dynamic myocardial perfusion imaging with second-generation dual-source CT: comparison with conventional catheter coronary angiography and SPECT nuclear myocardial perfusion imaging. AJR Am J Roentgenol. 2012; 198(3):521–529. [PubMed: 22357991]

106. Pijls NH, Fearon WF, Tonino PA, et al. Fractional flow reserve versus angiography for guiding percutaneous coronary intervention in patients with multivessel coronary artery disease: 2-year follow-up of the FAME (Fractional Flow Reserve Versus Angiography for Multivessel Evaluation) study. J Am Coll Cardiol. 2010; 56(3):177–184. [PubMed: 20537493]

107. Meijboom WB, Van Mieghem CA, van Pelt N, et al. Comprehensive assessment of coronary artery stenoses: computed tomography coronary angiography versus conventional coronary angiography and correlation with fractional flow reserve in patients with stable angina. J Am Coll Cardiol. 2008; 52(8):636–643. [PubMed: 18702967]

108. Koo BK, Erglis A, Doh JH, et al. Diagnosis of ischemia-causing coronary stenoses by noninvasive fractional flow reserve computed from coronary computed tomographic angiograms. Results from the prospective multicenter DISCOVER-FLOW (Diagnosis of Ischemia-Causing Stenoses Obtained Via Noninvasive Fractional Flow Reserve) study. J Am Coll Cardiol. 2011; 58(19):1989–1997. [PubMed: 22032711]

109. Min JK, Leipsic J, Pencina MJ, et al. Diagnostic accuracy of fractional flow reserve from anatomic CT angiography. JAMA. 2012; 308(12):1237–1245. [PubMed: 22922562]

110. Taylor CA, Fonte TA, Min JK. Computational fluid dynamics applied to cardiac computed tomography for noninvasive quantification of fractional flow reserve: scientific basis. J Am Coll Cardiol. 2013; 61(22):2233–2241. [PubMed: 23562923]

111. Min JK, Koo BK, Erglis A, et al. Usefulness of noninvasive fractional flow reserve computed from coronary computed tomographic angiograms for intermediate stenoses confirmed by quantitative coronary angiography. Am J Cardiol. 2012; 110(7):971–976. [PubMed: 22749390]

112. Einstein AJ, Henzlova MJ, Rajagopalan S. Estimating risk of cancer associated with radiation exposure from 64-slice computed tomography coronary angiography. JAMA. 2007; 298(3):317–323. [PubMed: 17635892]

113. Pearce MS, Salotti JA, Little MP, et al. Radiation exposure from CT scans in childhood and subsequent risk of leukaemia and brain tumours: a retrospective cohort study. Lancet. 2012; 380(9840):499–505. [PubMed: 22681860]

114. AAPM Position Statement on Radiation Risks from Medical Imaging Procedures. American Association of Physicists in Medicine; http://www.aapm.org/org/policies/details.asp?id=318&type=PP. Published 2011 [Accessed August 12, 2013]

115. Raff GL, Chinnaiyan KM, Share DA, et al. Radiation dose from cardiac computed tomography before and after implementation of radiation dose-reduction techniques. JAMA. 2009; 301(22):2340–2348. [PubMed: 19509381]

116. Willemink MJ, Leiner T, de Jong PA, et al. Iterative reconstruction techniques for computed tomography part 2: initial results in dose reduction and image quality. Eur Radiol. 2013; 23(6):1632–1642. [PubMed: 23322411]

117. Mayo J, Thakur Y. Pulmonary CT angiography as first-line imaging for PE: image quality and radiation dose considerations. AJR Am J Roentgenol. 2013; 200(3):522–528. [PubMed: 23436840]

Figure 1.

CT angiography evolution. **(a)** Renal arterial CT angiogram obtained in December 1991. Nine centimeters of longitudinal coverage required a 30-second spiral scan using 3-mm beam collimation. At that time, shaded surface displays were the only means for 3D display. Maximum intensity projection and volume rendering required offline processing, the latter on highly specialized computing systems. (Reprinted, with permission, from reference 13.) **(b)** With the introduction of four-row multidetector CT in 1998, it was possible to image the entirety of the aortoiliac system from thoracic inlet through the inguinal canal in a single acquisition. This volume-rendered CT angiogram was acquired in 28 seconds using a 4 × 2.5-mm helical scan and illustrates a calcified aortoiliac atheromata and an infrarenal

abdominal aortic aneurysm. (Reprinted, with permission, from reference 8.) **(c)** Volume-rendered CT angiogram acquired in 2001 with a single 21-second 16 × 1.25-mm helical scan encompasses the arterial system from extracranial circulation through pedal arteries. The speed of acquisition increased approximately 25-fold over the 10 years since the first spiral CT angiogram in 1991.

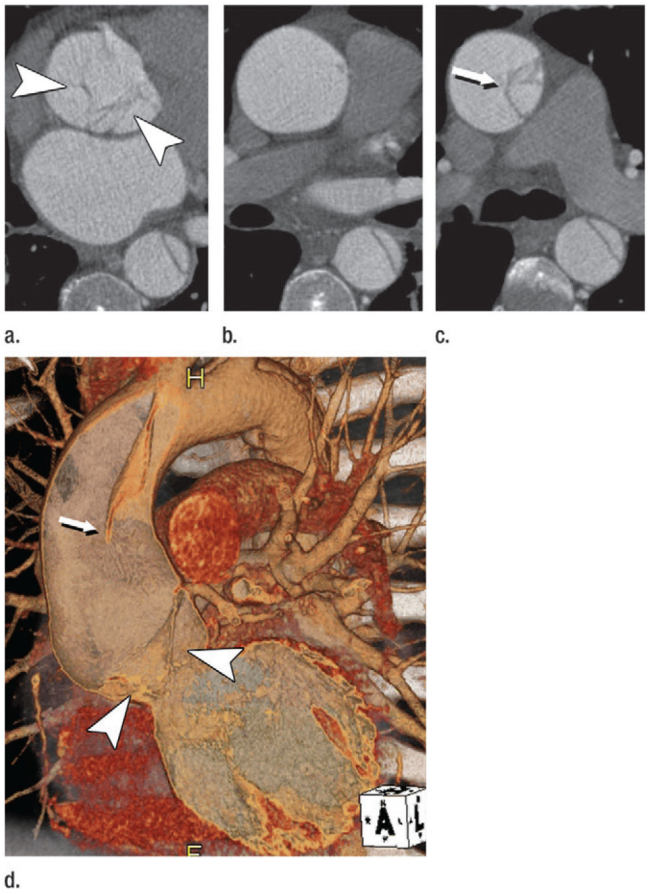

Figure 2.

Acute type A dissection in a 45-year-old man. **(a–c)** Transverse CT images show **(a)** irregular linear opacities (arrowheads) at the level of the aortic root, **(b)** no dissection flap in the mid ascending aorta, and **(c)** a dissection flap (arrow) between a true and false lumen in the distal ascending aorta. **(d)** Volume-rendered image depicts an extensive dissection, with proximal portion of dissection flap torn off and prolapsing onto and through the aortic valve (arrowheads). Arrow = dissection flap in the distal ascending aorta. In the absence of ECG-gating these nuanced findings would not be visible. (Reprinted, with permission, from reference 30.)

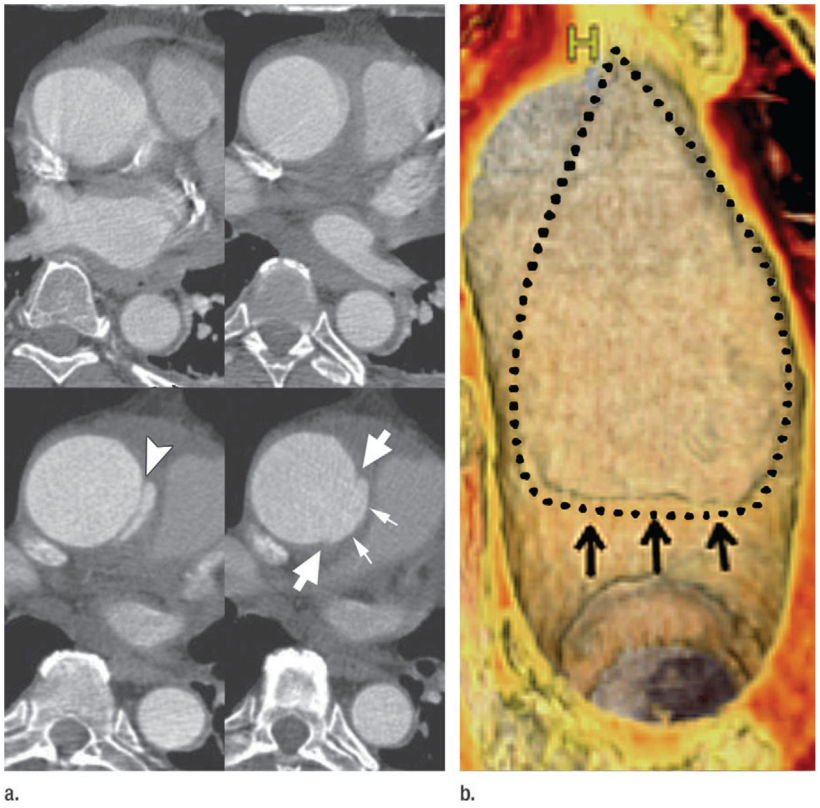

Figure 3.

Limited intimal tear of the ascending aorta. **(a)** Top: CT angiograms acquired without ECG gating show motion-related irregularity and blurring of ascending aorta. Bottom: ECG-gated CT angiograms obtained 12 hours later reveal an intimal flap in the proximal ascending aorta (arrowhead) consistent with an undermined edge of a limited intimal tear. Immediately superior, the edges of the limited intimal tear (large arrows) and bulging of the disrupted aortic wall (small arrows) are evident. These subtle details are not visible without ECG gating. **(b)** Volume rendering shows the luminal side of the 6-cm-long lesion. A small undermined flap (arrows) indicates the beginning of the tear, which extends superiorly into the proximal arch. Dotted line = borders of the tear. (Reprinted, with permission, from reference 24.)

Figure 4.

Rupturing aortic aneurysm with IMH. **(a)** Transverse nonenhanced CT sections demonstrate a 6-cm descending aortic aneurysm *(A)*. IMH (open arrow) is present at inferior margin of the aneurysm associated with displaced intimal calcification (thin arrow) and directly contiguous with hemorrhage in the middle mediastinum (thick arrows). **(b)** Oblique thin-slab MIP of a CT angiogram shows the IMH (open arrow) at the inferior margin of the aneurysm *(A)* and the long track of blood (solid arrows) extending through the mediastinum and into the pleural space where a large hematoma *(H)* occupies nearly half of the right hemithorax and is distinct from lesser-attenuating pleural fluid and enhanced atelectatic right lung. (Reprinted, with permission, from reference 24.)

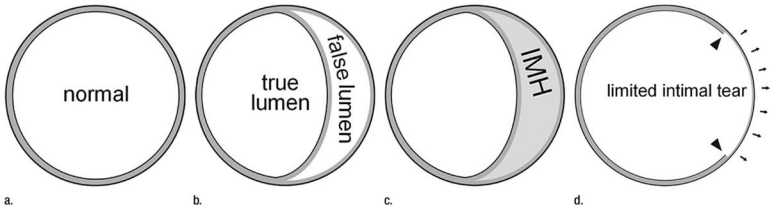

Figure 5.

Schematic of aortic dissection variants. **(a)** The layers of the normal extrapericardial thoracic aortic wall consist of the intima, the media, and the adventitia. Most of the substance of the aortic wall is media (gray). Both the intima and the adventitia (drawn schematically as black inner and outer contours of the aortic wall) are not visible at CT. All dissection variants have abnormal media in common. **(b)** Classic aortic dissection occurs within the outer third of the medial layer, resulting in two channels of blood flow. Note that the tissue separating the true and false lumen is mostly made of media tissue, and correctly should be termed the intimomedial flap (in lieu of intimal flap). **(c)** When the separation plane within the media is filled with stationary blood, instead of flowing blood, this is an IMH. **(d)** A limited intimal tear is a partial thickness tear (arrowheads) through the intima and inner portion of the media, exposing the residual media/adventitia, which tends to “bulge out” (arrows) relative to the remainder of the aortic circumference. (Reprinted, with permission, from reference 30.)

Figure 6.

Images in a 19-year-old basketball player with pain in legs when running the court. Diagnosis at CT angiography is popliteal entrapment syndrome. **(a)** Volume-rendered CT angiogram obtained in forced plantar flexion against resistance (stress) demonstrates occlusions of the popliteal arteries bilaterally (arrows) with minimal opacification of the crural arteries distally. **(b)** Volume rendering of same data as in **a** using an alternate opacity transfer function displays the lower leg muscles. The popliteal arteries are obscured but arrows mark their identical position as in **a**, indicating a medial course relative to the medial heads of the gastrocnemius muscles. **(c)** Volume-rendered CT angiogram in relaxed, neutral position demonstrates normal-appearing popliteal and crural arteries. **(d)** Stress and **(e)** relaxed views show the aberrant medial course of popliteal arteries (arrows) relative to the medial heads of the gastrocnemius muscles bilaterally (*).

Figure 7.

Right lower extremity ischemia with gangrenous toes. **(a)** MIP and **(b)** multipath curved planar reformation from lower extremity CT angiogram depict extensive bilateral atherosclerotic disease. Arterial supply to the right lower extremity is severely compromised by 3-cm-long common iliac artery occlusion (1), 2-cm-long high-grade stenosis of the external iliac artery (2), and proximal through midsuperficial femoral artery stenoses (curved arrow with 5-cm-long occlusion) (3). Right posterior tibial artery is occluded at its origin, but is reconstituted by the peroneal artery above the ankle (4), resulting in two-vessel runoff across the ankle. Arterial supply to the left lower extremity is compromised by a 75% stenosis of the proximal common iliac artery (5), greater than 90% stenoses of the external iliac artery (6, 7), 3-cm-long midsuperficial femoral artery occlusion (8), and moderate distal superficial femoral artery stenosis (9). Left anterior tibial artery is occluded 10 cm distal to

its origin but is reconstituted by the peroneal artery above the ankle (11) to provide two-vessel runoff across the ankle. Legions obscured on MIP by heavy arterial wall calcifications (1, 2, 5, 6, 7) are not obscured by calcium and better displayed on the multipath curved planar reformation. Because the displayed plane of a curved planar reformation is always through the vessels of interest, the representation of nonvascular structures may not follow standard anatomic relationships. An example of this is the ovoid opacities lateral to the popliteal artery, which represent portions of the lateral femoral condyles and lateral aspect of the tibial plateaus.

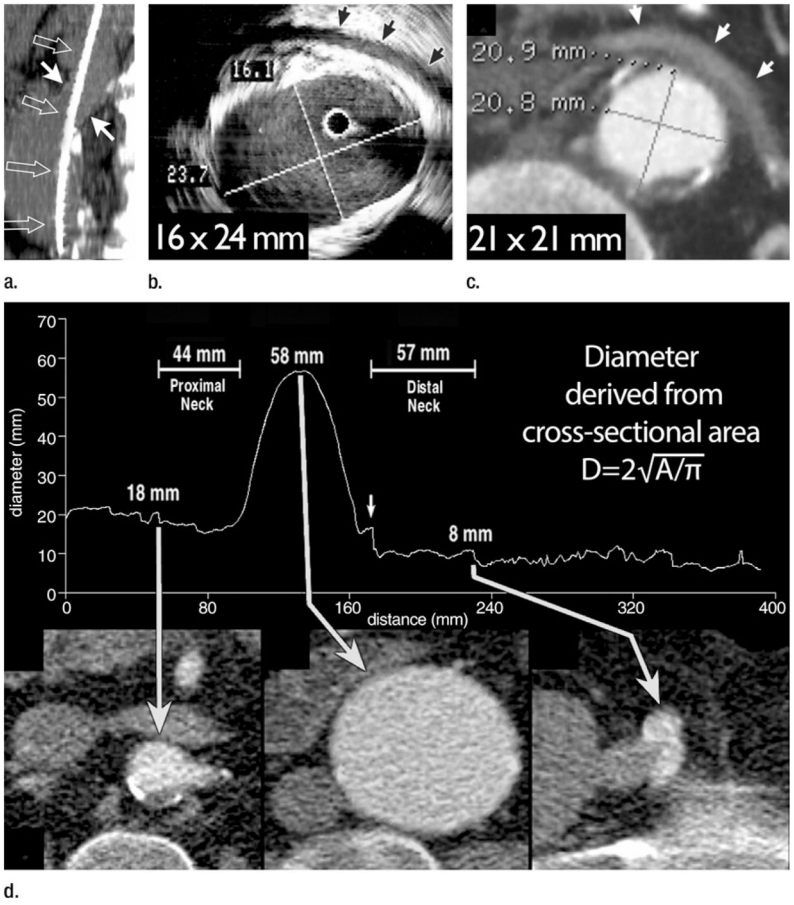

Figure 8.

(a) Sagittal 1.5-cm-thick MIP through an abdominal aortic aneurysm (AAA) depicts an oblique course of intravascular US catheter (open arrows) through the proximal aneurysm neck (solid arrows). A mean intravascular US catheter obliquity of 21.1° ± 2.6 relative to median axis of proximal neck lumen explains the tendency of intravascular US to depict greater eccentricity and maximal transverse diameter of the AAA neck relative to orthogonal CT sections. **(b)** Intravascular US and **(c)** double oblique CT reformation orthogonal to median axis of the lumen at level of the anticipated proximal fixation site for a stent-graft. Arrows = left renal vein. Aortic eccentricity is 0.68 for intravascular US and 1.00 for CT. Although intravascular US catheter obliquity may be the cause of some major axis overestimation, US artifacts substantially hinder confident wall identification. Note the distance between perceived anterior wall of the aorta and left renal vein on US image. CT image demonstrates that the majority of these high-level echoes are artifacts. **(d)** Following automated extraction of the median centerline of the aorto-right iliac lumen, oblique reformations are generated every millimeter along length of the centerline. The average diameter derived from cross-sectional area is plotted relative to longitudinal position along the centerline. CT sections correspond to the positions indicated by arrows on the plot. A small localized peak in the curve indicates origin of right and inferior-most renal artery (left arrow). Diameter immediately distal to this peak is 18 mm, corresponding to proximal stent-graft fixation site. Middle long arrow indicates maximum aneurysm diameter, which is 58

mm. Transition from aorta to right common iliac artery is apparent from an abrupt transition in cross-sectional area (short arrow). Further reduction in diameter indicates the origin of the right external iliac artery, which is 8 mm at its origin (right long arrow). In addition to providing measurements of diameter, distance along the path is readily ascertained, providing information on aortic segment lengths. (Part **d** reprinted, with permission, from reference 66.)

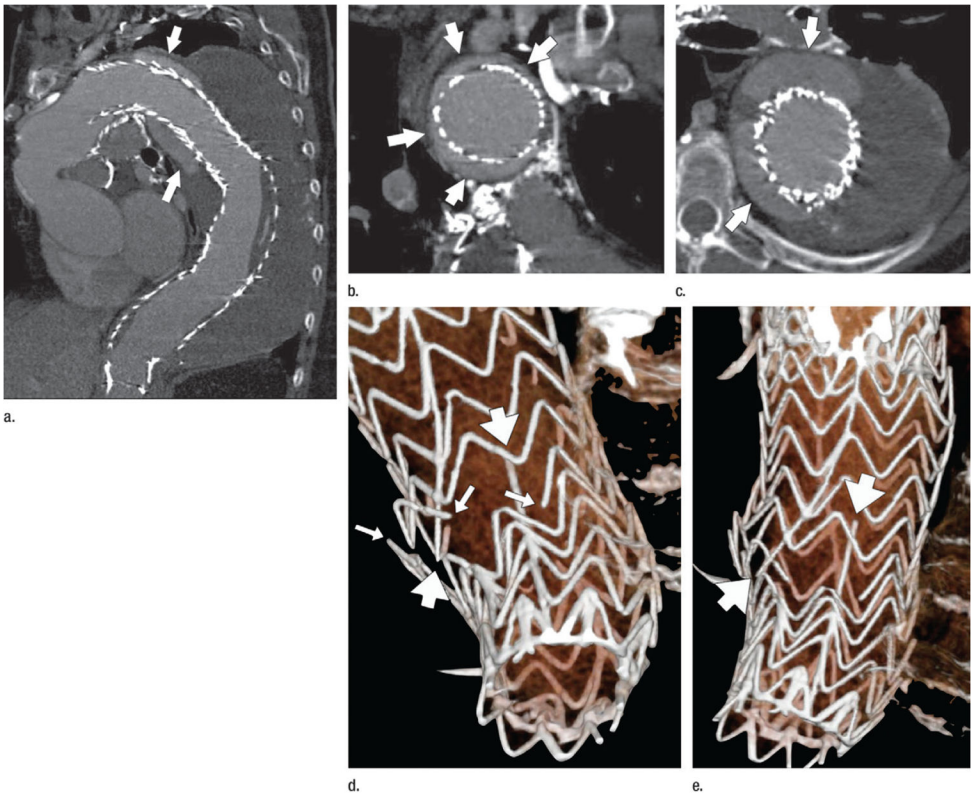

Figure 9.

CT angiography performed 1 year after deployment of a stent-graft to treat a descending thoracic aortic aneurysm. **(a)** Curved planar reformation demonstrates the proximal aspect of the stent-graft displaced from the lesser curve of the distal aortic arch, allowing contrast-enhanced luminal blood to flow around the stent-graft initially, inferiorly, and then in a spiraling direction distally (arrows). **(b)** Coronal oblique reformation through the distal aortic arch demonstrates poor fixation of the stent-graft at this level, with the endoleak channel filling over the majority of the aortic circumference (arrows). **(c)** Transverse section through a 9-cm descending aortic aneurysm (the aneurysm had measured 7 cm at the time of stent-graft deployment). Arrows mark the endoleak within the aneurysm sac. **(d, e)** Volume-rendered images of the distal stent-graft illustrate multiple fractures of the transverse stent rings (thin arrows) and the distal longitudinal strut (thick arrows). The ends of the fractured strut and rings are highly distracted, suggesting substantial motion and loss of structural integrity on the distal device, possibly leading to migration of the proximal device and the subsequent type IA endoleak and aneurysm expansion. (Reprinted, with permission, from reference 24.)

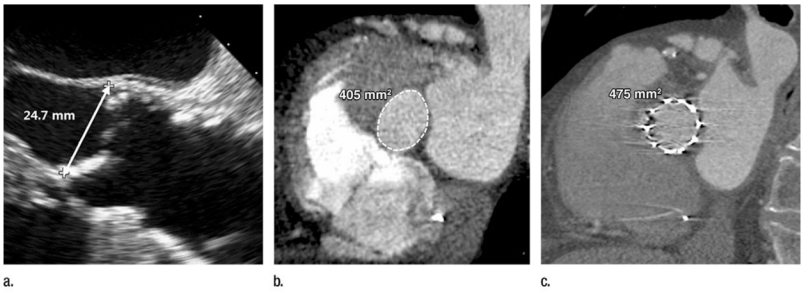

Figure 10.

(a, b) Images obtained before TAVR with **(a)** transthoracic echocardiography and **(b)** multidetector CT in an 84-year-old man with severe symptomatic aortic stenosis. The annulus measured 24.7 mm at two-dimensional echocardiographic assessment, resulting in a 26-mm transcatheter heart valve being selected (5.31 cm^2), despite the annulus measuring 4.0 cm^2 at CT, which would typically result in a recommendation of a 23-mm transcatheter heart valve. **(c)** The postdeployment CT image shows a circular but incompletely expanded transcatheter heart valve, owing to the significant oversizing of the valve based on the single two-dimensional measurement of an elliptical structure.

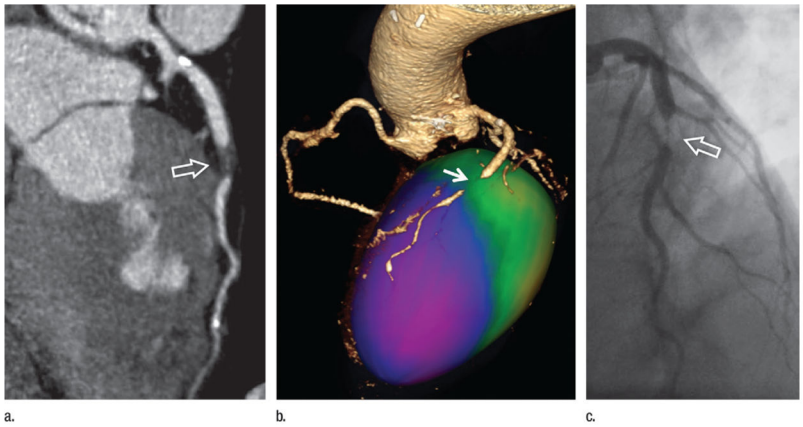

Figure 11.

Images in a 63-year-old man with treated hypertension and hyperlipidemia presenting with diffuse chest pain and shortness of breath. Conventional angiography findings 2 years earlier had been normal. **(a)** ECG-gated CT angiogram displayed with curved planar reformation demonstrates extensive noncalcified plaque in the mid–left anterior descending coronary artery, causing severe stenosis (arrow). **(b)** Color-encoded mapping of regional myocardial wall motion obtained from 10 reconstructions across the cardiac cycle establishes the functional consequences of the coronary lesion with hypokinesis (purple) in the anterior and apical left ventricle (arrow). **(c)** The coronary lesion (arrow) was confirmed on a subsequent conventional angiogram.

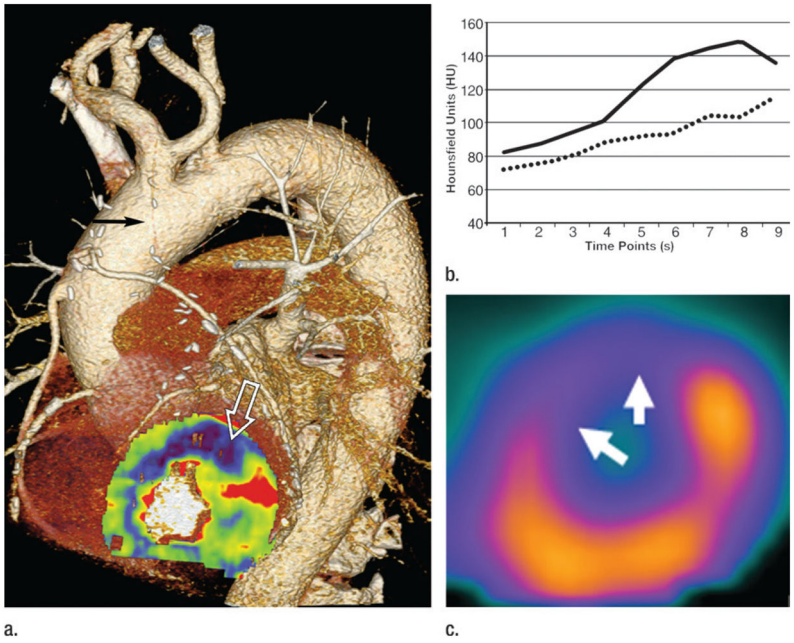

Figure 12.

Images in a 71-year-old man with CAD, status post three-vessel coronary artery bypass graft procedure and recurrent angina. **(a)** Pharmacologic stress, time-resolved myocardial CT perfusion maps superimposed on anatomic coronary CT angiography study demonstrates an occluded left internal mammary artery graft to the left anterior descending coronary artery (black arrow), with an associated stress-induced perfusion deficit in the anterior left ventricular myocardium (white open arrow). **(b)** Attenuation values within healthy (solid line) and diseased (dashed line) myocardium across the duration of the CT perfusion examination show persistently lower enhancement in the ischemic myocardium. **(c)** The perfusion deficit shown with CT correlates well with pharmacologic stress SPECT study in the same location (arrows).

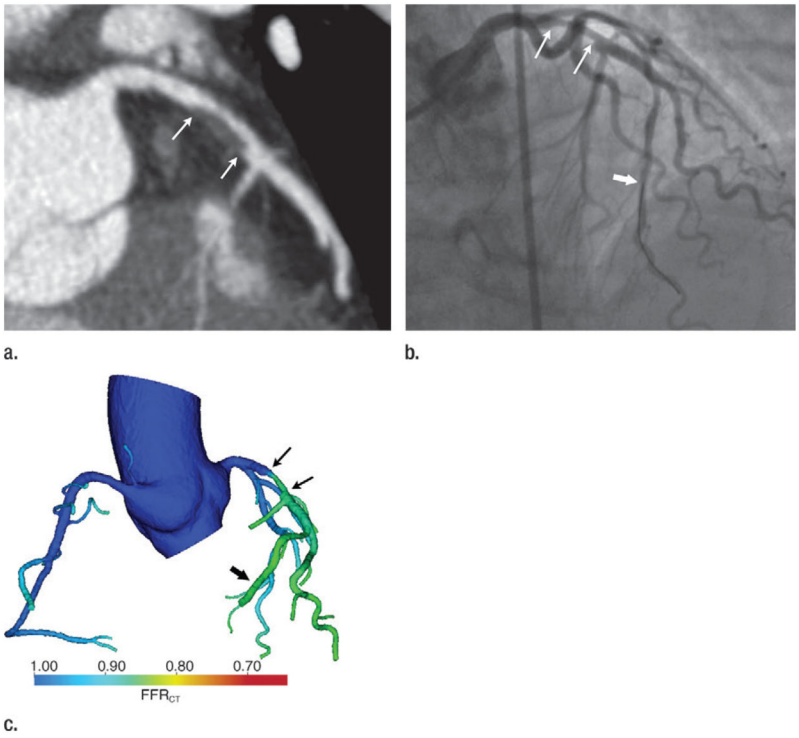

Figure 13.

Images in a 70-year-old woman with chest pain. **(a)** Coronary CT angiogram demonstrates a 50%–70% left anterior descending (LAD) coronary artery stenosis (arrows). **(b)** Coronary angiogram demonstrates the LAD stenosis (thin arrows), which was measured to be 58% at quantitative coronary angiography. FFR was measured to be 0.88 with a pressure sensor in the distal LAD during adenosine-induced hyperemia (thick arrow), indicating lack of functional (hemodynamic) significance. **(c)** Color encoding of computed FFR_{CT} values mapped to volume-rendered CT angiogram shows the LAD stenosis (thin arrows). The FFR_{CT} is 0.85 distal to the stenosis (thick arrow) at the site of the FFR measurement performed in **b**.

Table

Acute Aortic Syndromes

Group	Description
1	Dissection complex: aortic dissection and variants (diseased media)
1a	Classic aortic dissection*
1b	IMH
1c	Limited intimal tear (limited dissection)*
2	PAU (diseased intima)*
3	Rupturing aortic aneurysm*

* Lesions can occur without or without associated IMH.